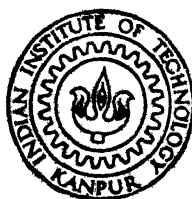# PREPARATION AND CHARACTERIZATION OF ELECTRON BEAM EVAPORATED INDIUMOXIDE FILMS

by

N. S. BABU

DEPARTMENT OF MATERIALS SCIENCE

INDIAN INSTITUTE OF TECHNOLOGY KANPUR

SEPTEMBER, 1982

PREPARATION AND CHARACTERIZATION OF ELECTRON BEAM EVAPORATED INDIUMOXIDE FILMS

A Thesis Submitted
In Partial Fulfilment of the Requirements
for the Degree of

MASTER OF TECHNOLOGY

by

N. S. BABU

to the
DEPARTMENT OF MATERIALS SCIENCE
INDIAN INSTITUTE OF TECHNOLOGY KANPUR
SEPTEMBER, 1982

MS-1982-M-BAB-PRE

CERTIFICATE:

This is to certify that the thesis entitled "Preparation and Characterization of Electron Beam Evaporated Indium Oxide Films" by N. S. Babu is a record of work carried out under my supervision and has not been submitted elsewhere for a degree.

(Dr. S. Kar)
Professor
Department of Electrical Engg.
and
Materials Science Programme,
Indian Institute of Technology, Kanpur
KANPUR

September 16, 1982.

ACKNOWLEDGEMENT:

I take this opportunity to express my most sincere thanks to Dr. S. Kar, who did more than simply guiding me through the course of this work. But for his constant interest in the problem and help in the experimental work, the work presented here would not have been complete. Also discussions with him on various points were of immense help and many of the conclusions arrived at in the present work are an outcome of these discussions. My association with Dr. Kar during the course of present work has been rewarding since this has also given me a feeling of the art of semi-conductor device fabrication.

I specially thank Dr. K.V. Rao for his generous help and cooperation through out the course of experimental work. I would thank Dr. T.R. Ramachandran for his help in TEM analysis. I also thank Mr. S. Varma for his frequent help during the writing of the thesis. I wish to express my sincerest thanks to Mr. Y. Ravishanker for his cooperation through out my work.

I am very thankful to Mr. S.R. Bhardwaj for his neat and efficient typing.

I am also thankful to all my friends who made my stay at I.I.T. Kanpur a pleasent one.

N.S. BABU

TABLE OF CONTENTS

Notations

A   Active area of the cell, (cm^2)

A*   Effective Richardson's Constant, $(A/cm^2 \, {}^\circ K^2)$

B   Constant, (K^{-1})

C   Total device capacitance, (F/cm^2)

d_{hkl} Interplanar spacing, $(\mathring{A})$

E_c Conduction band edge, (eV)

E_{FS} Fermi level in Si, (eV)

E_v Valence band edge, (eV)

h   Planck's constant, (erg. sec.);

         Index of the plane

I   Device current, (A)

I_D Diode current, (A)

I_o Diode saturation current, (A)

J_D Diode current density, (A/cm^2)

J_o Diode saturation current density, (A/cm^2)

J_{sc} Short circuit current density of the cell, (A/cm^2)

k   Index to the plane;

         Boltzmann's constant, $(eV/^\circ K)$

l   Index to the plane;

         Carrier mean free path, (cm)

L_D Debye length; cm

N_{doping} Doping density in Si; cm^{-3}

N_A, N_D Density of acceptors, donors in Si; cm^{-3}

N_{EDS} Effective density of states in Si band; cm^{-3}

N_{is} Density of interface states; $cm^{-2}v^{-1}$

n_i Intrinsic carrier concentration; cm^{-3}

n_{no}, n_{po} Equilibrium electron concentration in n-Si, p-Si; cm^{-3}

n_s Concentration of electrons at interface; cm^{-3}

P_{no}, P_{po} Equilibrium hole concentration in n-Si, p-Si; cm^{-3}

P_s Concentration of holes at interface; cm^{-3}

Q Charge; C

q Electronic charge; C

R Series resistance depicting the isolation of the interface minority carriers from the carriers in the bulk Si; Ohm.

R_{is}^{maj}, R_{is}^{min} Equivalent resistance for charge exchange between interface states and interface majority, minority carrier concentration; Ohm.

T Absolute temperature; °K

t_{ox} Oxide thickness; cm

V Applied d.c. bias; V

V^{FB} Flat band voltage; V

V_G Band gap potential in Si; V

V_{ox} Oxide voltage; V

$\bar{v}$ Average thermal velocity of free electrons; cm/sec.

Y Measured admittance of the device; mho

B q/kT; V^{-1}

F   Poition of Fermi level; V

n' p   Position of Fermi level in n- , p-Si;V

B   Potential difference between E_F and E_i;V

s   Surface potential in Si; V

ox' s   Permittivity of oxide, Si; F/cm

s' TC   Electron affinity in Si, transparent conductor, V

n 'p   Interface state capture cross section for electrons, holes; cm^2

$_R maj$,$_R min$ Interface recombination time constant for majority, minority carriers; sec.

Angular frequency; Hz.

ABSTRACT:

Transparant conductors are a relatively new class of compounds, having properties which can be exploited in a number of electronic devices. In_2O_3 films were evaporated by electron beam evaporation on silicon and fused silica substrates. Experimental set up has been developed for evaporating the electron beam evaporated films. It includes designing and assembling of the substrate holding arrangement, substrate heating arrangement, shutter arrangement, laying the gas line for purging the water and laying of chilled water line for cooling the electron gun crucible. Substrate heating at 300°C has resulted in getting good quality films. Film thickness was about 1100Å as observed by the interference color of the film. The conductivity type of all the evaporated films was stronglyn-type. Sheet resistivities of the films were measured using 4 point probe method. Photovoltage measurements were taken for the films evaporated on silicon substrate. Significant photovoltage was observed on n-type silicon, compared to none observed on p-type silicon. This is in contrast to the sputtered films. Hence, large barrier heights are obtained on n-type silicon in the case of electron beam evaporated films. X-ray structural characterization showed the presence of second phase elements in the In_2O_3 film. Second phase elements present were Sn_3O_4 and SnO_2. TEM characterization showed the polycrystalline nature of the film.

Annealing at 300-400°C in the oxygen ambient has improved the transparancy of the In_2O_3 film. Transparancy was about 92% in these films after annealing. Sheet resistivities obtained were in the range of 124-90   . Variation in the sheet resistivity for the films having equal thickness, may be attributed to the variation in the annealing parameters.

———————— —

I. INTRODUCTION:

1.1 Transparant Conductors:

Transparant conductors are relatively new class of compounds, having properties which can be exploited in a number of electronic devices[1]. These transparant conductors are incorporated with two diagonally opposite properties viz., transparancy and conductivity. They are transparant over most of the visible spectrum. The optical transparancy is because of its large band gap in the range of 3.5 to 4.0 eV and electrical conductivity is attributed to the presence of oxygen vacancies and substitutional impurities. These materials are similar to metals as far as conductivity is concerned with intrinsic carrier density of $10^{21}/cm^3$. Resistivities of these materials will be in the order of 10^{-4} Ohm-cm. Indium/oxide, Indium tin oxide and tin/oxide (SnO_2) are some of the transparant conductors.

Most of these oxide semiconductors are stable under typical environmental conditions, are resistant to chemical attack and adhere well to many substrates. These compounds have an useful property of forming a rectifying electrical barrier with semiconductors such as silicon.

Transparant conductors are used in :

1. wind screens for deicing and defogging;

2. transparant electrodes in L.C.D., where one of the electrodes is transparant;

3. in optoelectronics for heterojunctions.

1.2 Methods of Deposition of Transparant Conductors:

There are various methods of depositing transparant conductors such as electron beam evaporation, R.F. sputtering, spray hydralysis and chemical vapor deposition. Here special emphasis is given about electron beam evaporation.

1.3 Electron Beam Evaporated Films:

Electron beam evaporation is also one type of thermal evaporation but having an edge over resistive heating. Simple resistive heating of an evaporation source suffers from the disadvantages of possible contamination from the support material and the limitations of the input power which make it difficult to evaporate high melting point materials. These draw backs can be overcome by an efficient source of heating by electron bombardment of the material. In principle, this type of source is capable of evaporating any material[2].

Ability of concentrating energy over small areas by means of focussing electron beam has led to this powerful technique of material preparation. The Kinetic energy of the focussed electrons impinging[3] on the surface of the evaporant is transformed into thermal energy upon impact and the temperature of the nearby atoms or molecules is raised above their vaporization point. Heating of the evaporant is controlled by the density of the electron beam and electron velocity.

Various advantages offered by this technique are[4]:

1. Only a small area is heated and hence outgassing is reduced;

2. Source container is not heated and contramination
    from the source is further minimized by water cooling
    the e-gun crucible;

3. Higher temperature generated at the focal point of
    an electron beam permits rapid evaporation of high
    melting point materials;

4. Evaporation rate can be controlled easily.

Devices operating on the principle of electron-bombardment
heating are refered to as electron guns[5]. Many varities of
electron beam source designs are being used by the Reserchers.

(a) **Work accelarated electron guns:**

Work accelarated structures have a hot cathode
in the form of a wire loop in close proximity to the
evaporant. Electrons converge radially upon the work and
the simplest arrangement is pendent drop configuration.

(b) Self accelarated electron guns:

This class of guns are similar to X-ray tubes.
A small tungsten helix or hairpin filament constitutes
the electron source. Focussing is achieved by electrostatic
shield surrounding the filament and evaporant.

The ease with which an electron beam can be deflected
by a magnetic and/or electrostatic field may be exploited
to scan or to program the same beam to perform sequential
deposition from different source materials.

In thin film vacuum deposition methods electron beam
evaporation claims highest film purity compared to other
methods.

By using 6Kw, 180° bent beam gun, Edwards and Graper[6]
have determined the deposition rate, required beam power,
charge material form and suitability of evaporation for
different materials. It was found that the deposition rate was
influenced by the variable characteristics of the electron
beam gun parameters and evaporability of the material by
charge material form. For melting materials, those which
melt before evaporability eg: Al, the rate increases with
increased power density (decreased spot size) on the melt,
with semi melting materials (those which melt only in beam)
eg: Sapphire and sublimating materials eg: SiO, which are not
able to absorb the full power of the beam, the power and rate
can be increased only by increasing the spot area.

Charge form affected only the evaporability of the
materials tested and not the deposition rate. Materials that
are good thermal conductors and melt well below evaporation
temperature eg: Zinc, can be evaporated from any form or raw
material. All other materials are difficult or impossible to
evaporate from anything but chunks or hot pressed pieces.
These materials when heated as granules or powders, form a
localized hot spot of very small volume at too low a power to
permit significant evaporation. The large surface area of
granules and powders also permits the absorption of water and
other contaminants which are released upon heating, causing
localized exploding from the gun.

Most materials were not able to absorb all the power

available from the power supply and increasing the power above what can be absorbed caused spitting and film pinholing. If the energy density exceeds that which can be stably dissipated, explosive instabilities occur, cause spitting. The rate can be increased by increasing the spot size, thereby reducing the energy density and allowing a further/in beam power. The spot area can be increased by sweeping the beam rapidly or by changing the gun focus or both. For SnO_2 preferential form suggested was hot pressed form with a beam power of 0.5 KW.

The relationships between microhardness, density and composition of silica films prepared by resistance heating and by electron beam evaporation were compared by S. Furuchi et.al.[7] It was observed that the hardness of the film prepared by electron beam evaporation is higher than that of the resistance heating evaporation. Experimental data for the dielectric properties of Yb_2O_3 films deposited by electron beam evaporation exhibited[8] better dielectric properties such as relatively high dielectric constant, a low dissipation factor and high break down field strength.

Evaporation studies made by Hoffman et.al.[9] by electron beam evaporation of hot pressed Al_2O_3 have showed that electron beam evaporated films onto the silicon substrate are oxygen deficient due to the dissciation of Al_2O_3. Stoichiometry Al_2O_3 films can be obtained with the confinement of the evaporant and reactive ambient in chamber below the substrate. Several ambient parameters such as substrate preheating, substrate temperature during evaporation and rates of

evaporations were made to obtain their effects on film
properties. Evaporation studies were carried out in wet
oxygen ambient and dry oxygen ambient. It appears from
measurements, silicon is either reacting with the growing film
or it becomes a catalyst for Al_2O_3 growth in the wet oxygen
system. Oxide films deposited in wet oxygen system exhibited
greater granularity at the silicon film interface than the
films deposited in dry oxygen. Further greater uniformity
over the substrate surface for films deposited in dry atmosphere
was observed. The fact that the etch rate of the films deposi-
ted in dry oxygen are slower than the etch rate of films
deposited in wet oxygen, indicated that the density of the films
deposited in dry ambient is greater than that for corresponding
films in wet oxygen system. Flat band voltage was observed
to be dependent on the substrate temperature. Breakdown
fields in excess of 10^6V/cm were exhibited in dry oxygen
ambient.

In continuation of their study same authors have
explored that the electrostatic charges developed on the
substrate during electron beam deposition process play a
significant role[10] in effecting the electrical and physical
film properties. These investigations indicated that the
build up alters both the electrical and optical properties
of the Al_2O_3 films. Copper shield grounded to the base plate
and placed over various positions of the electron beam gun
provided effective control over substrate potentials. Al_2O_3
films varying in shades off brown to completely clear are :

produced by altering the electrostatic fields from -22V (for the the darkest films) measured between substrate and ground to less than -2V between the substrate and ground (for clearest films). Films were produced between 1000 and 1500 $\overset{o}{A}$ thick and uniform within 200$\overset{o}{A}$ across 5.02 cms silicon wafer. Large negative voltage shifts were measured on p-type silicon prior to annealing with C-V measurements.

1.4 Electron/X-Ray Damage of Electron-Beam Evaporated Films:

Edwards B Graper[11] has described the charged particle flux generated by electron beam deposition sources. These charged particles interact on the surface of thinfilms affecting their properties. These charged flux could originate from any of the following. (1) scattered electrons from the melt, (2) thermionic emission from the melt, (3) reflected electrons from the melt, (4) beam ionization in the evaporant cloud over the gun.

Based on theoritical calculations thermionic emission could not be a major source of flux and it would not account for over 0.01% of the measured flux at any reasonable temperature. Reflected electrons might be a major source of flux in relation to thinfilm evaporation. Yamagishi[11] has calculated, that the reflected electrons might contribute to 90% of the charged flux. Experimental results showed that the reflected electrons could not have that major contribution as reported by Yamagishi. This flux might be explained by the beam ionization of the evaporant over the gun. The evaporant

stream may be low density thermal plasma. The work of
Edwards B Graper is not complete, as it is unable to give the
clear cut amount of different charged fluxes.

Schvermeyer has reported pronounced non-uniformity
in films of Ta[12] deposited by electron beam evaporation.
Different effects were considered as possible causes for the
non uniformity of the films. It has been demonstrated that
during electron beam evaporation, high energy electrons are
reflected toward the substrate. These electrons cause
floating substrates to acquire high negative voltages. Positive
ions created during the eveporation were accelarated to the
substrate and cause sputtering of the deposited film. The
electric field produced by the high negative voltage of the
substrate and by the grounded mask causes these ions to crowed
toward the centre of the substrate. It was observed that the
sputtering was not caused by ionized residual gas.

Quantitative study of film thickness at various
substrate areas were conducted as a function of applied voltate,
using Multiple beam interferometry techniques. It was observed
that the centre of the film was thinner than the edges.

So far no effort was made to study the film defects
caused by X-rays on experimental basis. Characteristic X-rays
will be produced when electron beam impinges on the material.
When these X-rays strike the film surface, surface of the film
will be get damaged. It is very important to characterize the
X-ray damage to the film surface to understand the quality of
electron beam evaporated films.

1.5 Transparant Conductor Surface Barrier Devices and Interface States.

Interface states or surface states are defined as energy levels within the forbidden band gap at the insulator-semiconductor interface which can exchange charges with the semiconductor in a short time.[13] The origin of these states is yet to be known clearly. However it has been shown theoretically that whenever the periodic lattice structure of the crystal is interrupted these states will exist.[14-15]

Reliable data concerning interface states can be obtained using MOS structure. Transparant conductor-Oxide-Semiconductor (TCOS) structure closely resembles the Metal-Oxide-Semiconductor (MOS) structure.[16] If the transparant conductor is sufficiently conducting, its energy bands may be assumed to be flat as in a metal. Consequently, energy bands will bend in the semiconductor alone and the TCOS structure reduces to a surface barrier device and hence can be considered similar to MOS device. In the case of MOS structure measurements were carried out in dark only. But using TCOS structure, measurements were carried out recently using optical illumination.

TCOS structure has got the following advantages over MOS structure:

(1)   In this case optical illumination is employed;

(2)   Depositing transparant conductor, typically 2000Å thick is easier than to deposit semi transparant metal film;

(3) Semitransparant metal film will absorb considerable amount of light and these films are chemically and structurally unstable compared to the oxide films;

(4) For taking long measurements; TCOS structure has definite edge over the MOS structure because of its long durability.

Using thin oxides of the order of 0-400$\overset{o}{A}$, TCOS structure has been explored for investigating interfaces. In structures with such thin oxides, the quasi-static technique may not be feasible in view of large leakage currents. Low frequency device capacitance may not be attained in weak and strong inversion regimes without optical illumination.

1.6 Scope of the Present Work:

Mainly the work has been aimed at designing and assembling of the vacuum chamber parts for carrying out the electron beam evaporation. This includes the designing and assembling of the substrate heating arrangement, laying of the chilled water line for cooling the electron gun crucible and laying the gas line for purging the water. Then the work was to carry out the structural and electrical characterisation of the electron beam evaporated transparant conducting films. As revealed by the literature survey, form of the charge material to be evaporated is very important in the electron beam evaporation. Here tin doped indium oxide was taken in the tablet form. Electron beam evaporated films were annealed at different annealing temperature and annealing times to

study the effect of annealing on the transparency and
conductivity of the films. Sheet resistivities of the films
were measured using 4 point probe method. Photovoltage measure-
ments were done for the electron beam evaporated and sputtered
films deposited on n-type and p-type silicon substrates.
Structural characterization by X-ray and TEM was performed.
X-ray characterization was performed to find the structural
defects of the film. TEM characterization was done for the
films at the different regions to find the structural defects
of the film; to find the grain size and to know the nature of
the film.

II THEORITICAL BACKGROUND:

2.1 Electrical Conduction In SnO_2:

SnO_2 has a rutile structure with its unit cell containing four oxygen and two tin atoms. The electrical properties of SnO_2 are isotropic inspite of its anisotropic crystal structure.

High conductivity of these films (transparant conductors) have been attributed to the presence of native defects such as oxygen vacancies, which contribute to donar levels to the material. These vacancies are incorporated either during film growth or after deposition by annealing the film in an inert atmosphere. The more oxygen that is removed from the film, the more metallic in character the film becomes upto the point of being an opaque metal film. Annealing at 700°C produced highly reduced opaque film. An optimum annealing temperature would be from 300°C to 400°C and would depend on film thickness. M. Nagasawa and S. Shinoyo[17] have studied[1] the heat treatment was to enhance oxygen vacancies or in other words to reduce the crystals. Annealing in H_2 above 900°C leads to the introduction of a new donar level at (50 ± 5) meV deep and which is deeper than the first oxygen level (34meV) The two donar levels at 34 meV and 140 meV were identified to be the first and second ionized states of oxygen vacancy.

Laja et.al[18] have investigated the chemical composition of thin nonstochiometric films of tin/oxide. The high value of the electrical conductivity of these films is caused by the existance of a donar level in the wide energy gap. The problem of whether the donar level is associated with oxygen vacancies in an oxygen sublattic or with the tin atoms in interstitials remain unsolved. From the composition and the stoichimmetry of the films under various technological conditions, it has been suggested that the electrical conductivity is caused by the vacancies in the oxygen sublattice. The donar level lies at 0.2-0.3 eV below the bottom of the conduction band, most of the donar centres are ionized.

2.2 Current Transport Mechanism In Heterojunctions:

2.2.1 Possible Transport Mechanisms:

In the case of heterojunctions or surface barrier devices such as MOS and SOS diodes, there can be number of carrier transport mechanisms which contribute to the diode current. In all these diodes, potential barrier is formed at the silicon surface. In SOS diodes, the interface states at the oxide-degenerate semiconductor band gap are localized while in the MOS diodes they are not localized. As far as the possible mechanisms of carrier transport in dark are concerned, these diodes hardly differ[19]. The energy band diagram of an SOS diode on n-type at a moderate forward bias is shown in Fig. 2.1. The possible carrier transport

mechanisms are thermionic emission (process a), thermonic
field emission (process b), field emission (process c),
recombination tunneling (process d), minority carrier
injeotion (process e) , recombination current (process f)
and multistep tunneling (19-20).

The relative magnitudes of these mechanisms depend
upon various parameters such as height of the potention barrier
$\emptyset_B$, density of interface states, device voltage V and
device temperature. An oxide layer of thickness less than
35Å is tunnelable to carriers. The effect of an oxide layer
on the transport mechanisms can be taken into account of an
oxide tunneling transmission coefficient. This will decrease
exponentially with increasing oxide barrier height and thickness
of the oxide.

Process (a) :

In thermionic mode of carrier transport, the
majority carriers overcome the silicon barrier by pure
thermionic emission and thereupon tunnel through the thin-
oxide layer. In this case the total potential barrier can be
treated seperately interms of the silicon barrier and an
oxide barrier. The resultant current density is determined
by multiplying the thermionic current over the silicon
barrier by tunneling transmission coefficient. The expression
for the thermionic-tunneling current density J_{TT} takes the
form[21].

$$J_{TT} = T_{ox} (V) J_o \exp \left(\frac{qV}{nkT} \right) \quad \ldots \ldots (2.1)$$

where T_{ox} (V) is the oxide tunneling transmission coefficient and n is the diode ideality factor. The expression for the diode saturation current density can be written as

$$J_o = A* T^2 \exp. (\frac{-q\phi_B}{KT}) \ldots (2.2)$$

Process (b) and Process (c):

Thermionic field emission is the likely mechanism at intermediate temperatures and field emission (process c) is important mechanism at low temperatures. Importance of the process (b) and process (c) would further extend in temperature at higher dopings i.e. at thinner barrier. Assessment of the process (b) and process (c) is based on the assumption of direct tunneling through the semiconductor barrier region.

Process (d):

Recombination tunneling (process d) is important mechanism at higher (room) temperature. It requires high density of gap states suitably located in energy. The transition of carriers from the silicon majority carrier band band into interface states by generation-recombination and then tunneling through the oxide into the metal causes an excess current. Recombination-tunneling current density can be written as [20]

$$J_{RT} = 4 \int_{E_v}^{E_c} \frac{N_{is}(E) \, dE}{T} \, dE \ldots (2.3)$$

It increases with the increase of interface state density and is controlled by oxide tunneling time $T = B.e \, {}^{t_{ox}}$ where B is constant and is a parameter which increases with the oxide barrier height.

Process (e):

Minority carrier injection dominates at intermediate voltage regime and it is likely the mechanism if the barrier height is sufficiently high to suppress the majority carrier flow. For this mechanism the current-voltage relationship can be written as

$$J_D = J_o \, \exp(\frac{qV}{nkt}) \quad \ldots\ldots \quad (2.4)$$

$$\text{where} \quad J_o \quad T^3 \, \exp(\frac{-E_g}{KT})$$

Process (f):

Recombination in the space charge region dominates at the low voltage regime.

These mechanisms from process(a) to process (f) as illustrated in Fig.(1) are usually associated with carrier transport across a surface barrier. This however is not an extensive list.

Multistep tunneling rather than the direct tunneling through the silicon barrier is a posibility at temperature higher than 300°K. Such a transport process gives the forward I_D - V characteristic a form represented by

$$I_D = I_o \, \exp(AV) \, \exp(BT) \quad \ldots \quad (2.5)$$

where A and B are constants. Multistep tunneling is a possible mechanism when there is (1) temperature independent slope of the $\ln I_D$- V plot, (2) a weak dependence of the diode current on temperature (T) , (3) a linear relation between $\ln I_o$ and T, and (4) a large decrease in the zero bias silicon band bending with temperature.

2.2.2 Identification of Dominant Transport Mechanisms:

It can be seen from the above discussion that the current-voltage characteristic of these diodes is most difficult to interpret. Several mechanisms can occur in parallel and it is very difficult to seperate and identify a dominant mechanism contributing to the diode current in a particular diode. An effective means to narrow down the possible dominant mechanisms is to measure the current-voltage and high frequency capacitance-voltage characteristics of the device over a wide range of temperature. In addition, - information about interface state density can be obtained from the small signal admittance-voltage characteristics in the forward bias regime. But this is probable only in thicker oxides. From forward current-voltage characteristics at different temperature, J_o can be obtained at each temperature by extrapolation of the linear region of $\ln J_D$-V characteristic to zero bias and plots of $\ln J_o$ as a function of T, $1/nT$ can be made. If thermionic emission of majority carriers over the top of the silicon barrier or minority carrier injection is to be the dominent mechanism, then one

obtains linear J_D-V characteristics over a wide range of
temperature with a temperature independent diode ideality
factor close to unity and a linear plot of ln J_o against
1/T . If at each temperature, the value of the barrier
height obtained from the $1/C^2$- V plot is close to the value
of the barrier height obtained from the activation energy
plot, and if it is much different from the bandgap, then
the thermionic emission is the most likely dominant mechanism.
In this case, nT is expected to be a linear function of T.
However, seperation between thermionic emission and minority
carrier injection becomes difficult, if the value of the
barrier height obtained from the activation energy plot is
not much different from bandgap. One can also obtain a
linear plot of lnJ_o against 1/T when recombination current[19,22]
dominates. But in this case, the value of the activation
energy obtained is very much different from E_g and is close
to E_g /2.

A linear ln J_D-V can also be obtained for thermionic
field emission, field emission or multistep tunneling
mechanisms. If the diode current is temperature dependent,
and if the plot of ln J_o against 1/nT is linear, then
thermionic field emission is the likely mechanism. In this
case nT is expected to be a nonlinear function of T at low
temperature. In case of field emission and multistep tunneling
mechanisms, dependance of the diode current on temperature
is negligible. For these mechanisms, the ln J_D-V plots at

different temperatures have equal slopes, and ln J_o varies

linearly with T. The distinction between these two mechanisms

becomes difficult at low temperatures. However at high

temperatures, field emission is not probable and multistep

tunneling can be expected to be the dominant mechanism. As

reported by S. Ashok et. al [23], same mechanism may not dominate

over the entire temperature range and there can be different

transport mechanisms in different temperature ranges.

2.3 Investigation of Interface States in TCOS Structures:

2.3.1 Effect of Interface States:

The existence of surface states was first found

experimentally by Shockley and Pearson in their surface conduc-

tance measurement. Surface states have been classified into

fast and slow states depending upon the time taken by them in

exchanging charges with the conduction or valance band of the

semiconductor. A surface state is considered as a donar state

if it can be neutral or it can become positive by giving up an

electron. For an acceptor surface state, it can be neutral or

it can become negative by accepting an electron. It has been

found that the interface states cause a bias shift and frequency

dispersion of the admittance curves. They also generate excess

currents and flicker noise, thus strongly influencing the

device performance.

2.3.2 Equivalent Circuits:

When an a.c. signal is super imposed on the d.c.

bias the surface levels will more up or down with the valance

and conductance bands when the fermi level remains fixed. A
change of charge in the surface state occurs when it crosses
the fermilevel. This change of charge will contribute to the
MIS capacitence and alter the ideal MIS curve. The basic
equivalent circuit incorporating the surface states is shown
in Fig. 2.2(a). In the figure, C_{ox} and C_{sc} are the oxide
capacitance and space charge capacitance respectively. The
product $C_{is} R_{is}$ is defined as the recombination time constant.

$$R = \frac{1}{\overline{V} - p_s} \qquad (2.6)$$

where $\overline{V}$ is the average thermal velocity; , capture cross
section of the states; p_s, the carrier concentration at the
interface.

The parallel branch of the equivalent circuit in
Fig. 2.2(a) can be converted into a frequency dependent
capacitance C_p in parallel with a frequency-dependent
conductance, as shown in Fig. 2.2(b) where,

$$C_p = C_{sc} + \frac{C_{is}}{1 + w^2 R_{maj}^2} , \quad \ldots\ldots (2.7)$$

and

$$\frac{G_p}{w} = \frac{C_{is} w R_{maj}}{1 + w^2 R_{maj}^2} , \quad \ldots\ldots (2.8)$$

where $w = 2\pi f$, f being the frequency of an a.c. signal.

2.3.3 Determination of Interface State Density By Capacitance Method:

When the frequency is small, all the states charge and discharge and the device will be a pure capacitor. At very low measurement frequencies ($w R_{is}^{maj} 1$) the resistance R_{is}^{maj} becomes very small and equivalent circuit can be approximated to Fig. 2.3(a). Thus the circuit becomes a purely capacitive one and the low frequency capacitance is given by:

$$\frac{1}{C_{LF}} = \frac{1}{C_{ox}} + \frac{1}{C_{sc} + C_{is}} \, ,$$

OR

$$\frac{1}{C_{LF}} = \frac{1}{C_{ox}} + \frac{1}{C_p} \, , \quad \ldots\ldots\ldots (2.9)$$

where $C_p = C_{sc} + C_{is}$.

When the frequency of the a.c. signal is very high ($w R_{is}^{maj} 1$), the interface states are not able to follow the signal and therefore do not contribute to the device capacitance. The equivalent circuit in this case reduces to Fig. 2.3(b).

Then the high frequency capacitance is given by:

$$\frac{1}{C_{HF}} = \frac{1}{C_{ox}} + \frac{1}{C_{sc}} \quad \ldots\ldots\ldots (2.10)$$

Using equations (2.9) and (2.10) we can evaluate C_p and C_{sc}.

(b) Evaluation of C_{ox}, T_{ox} N_{doping} and V_{FB} :

Oxide capacitance C_{ox}, can be easily found as the constant maximum capacitance in strong accumulation. Oxide thickness T_{ox}, can be expressed as:

$$T_{ox} = \frac{A\ E_{ox}}{C_{ox}} \qquad \ldots\ldots\ldots\ (2.1.1)$$

where A is the area of the device and E_{ox} is the permittivity of SiO_2.

The doping density in silicon can be found either from the slope of $1/C^2$-V plot or the maximum inversion capacitance C_{min} (the constant minimum capacitance in high frequency C-V plot)

Doping density N_{doping} can be expressed as,

$$N_{doping} = \frac{2}{q\ E_s}\ \frac{1}{slope}, \qquad \ldots\ldots\ldots (2.12)$$

where slope = $(\frac{d\ C^{-2}}{d\ V})$ A^2.

In the devices which have sufficiently thick oxide to sustain an inversion layer, the doping density can be computed using the constant minimum capacitance C_{min} of the high frequency C-V plot, with the help of the following equations:

$$\frac{1}{C_{min}^{sc}} = \frac{1}{C_{min}} - \frac{1}{C_{ox}}, \qquad \ldots\ldots\ldots (2.13)$$

$$C_{min}^{sc} / A = \sqrt{\frac{q\,E_s\,N_{doping}}{2\,(V_g - 2\phi_F)}} \quad , \quad \ldots\ldots\ldots (2.14)$$

$$\phi_F = \left(\frac{KT}{q}\right) \ln \frac{N_{EDS}}{N_{doping}} \quad , \quad \ldots\ldots\ldots (2.15)$$

where C_{min}^{sc} is the minimum space charge capacitance, V_g is the band gap of the semiconductor, ϕ_F is the seperation of fermilevel from the conduction band edge or valance band edge depending on whether the semiconductor is n-type or p-type; N_{EDS} is the effective density of states at the conduction/valance band edge in n/p-type semiconductor.

Space charge capacitance at flat band can be evaluated from the equation,

$$C_{sc}^{FB} = \frac{\sqrt{2}\,A\,E_s}{L_D} \quad , \quad \ldots\ldots (2.16)$$

where L_D is the Debye length and is given by:

$$L_D = \sqrt{\frac{2KT\,E_s}{q^2\,N_{doping}}} \quad . \quad \ldots\ldots\ldots (2.17)$$

Total capacitance at flat band (C^{FB}) can be obtained from the equation:

$$\frac{1}{C^{FB}} = \frac{1}{C_{sc}^{FB}} + \frac{1}{C_{ox}} \quad . \quad \ldots\ldots\ldots (2.18)$$

The flat band voltage V^{FB} can now be read from the high frequency C-V plot, corresponding to the value of C^{FB}.

(c) <u>Determination of $_s(V)$</u>:

The surface potential or band bending s can be determined as a function of bias voltage.

$_s(V)$ can be expressed as:

$$_s(V) = \int_{V^{FB}}^{V} (1- \frac{C}{C_{ox}}) \, dV \ldots\ldots (2.19)$$

This method is very accurate as characteristic is getting integrated and differentiation of the characteristic can introduce errors.

(d) <u>Determination of N_{is}</u>:

Using equations (2.9) and (2.10), one can evaluate C_p and C_{sc} respectively at various voltages and plot them as a function of surface potential. The value of C_{sc} in strong inversion can be calculated with the help of the following relation:

$$C_{sc} = \frac{A \, E_s}{L_D} \left[\frac{(e^{B\,s} - 1)+\frac{p_{no}}{n_{no}} (1- e^{-B\,s})}{(e^{B\,s} - B\,s -1)+\frac{p_{no}}{n_{no}} (e^{-B\,s}+ B\,s -1)} \right]^{1/2}$$

for n-type,

$$C_{sc} = \frac{A \, E_s}{L_D} \left[\frac{(1-e^{-B\,s}) +\frac{n_{po}}{p_{po}} (e^{B\,s}-1)}{e^{-B\,s} + B\,s-1) + \frac{n_{po}}{p_{po}}(e^{B\,s}-B\,s- 1)} \right]^{1/2}$$

for p-type. $\ldots\ldots\ldots$ (2.20)

where p_{no} and n_{po} are the minority carrier densities in n and p type respectively under equilibrium conditions, n_{no} and p_{po} are the majority carrier densities in n and p type respectively.

Difference of C_p and C_{sc} at any time gives the value of C_{is} at that particular point. The surface state density at the energy corresponding to that value of   s can then be determined by,

$$N_{is} = \frac{C_{is}}{q \, A} \, . \qquad \dots\dots\dots \quad (2.21)$$

3. Experimental Procedure:

3.1 Deposition Set Up:

All modern semiconductor devices need to be
fabricated very carefully and in ultra clean environment,
because of their small size and extreme suceptibility to
contamination. In a clean room the particle count is kept
below a specified maximum and air flow, temperature,
humidity and air pressure are regulated. For semiconductor
device fabrication, class 100 clean space is generally
recommended.

Electron beam evaporation was chosen as the
method of deposition of transparant conducting films. Varian
VT-112B ultrahigh vacuum system was used for carrying out the
deposition. The main work involved was installation of electron
beam gun; laying of chilled water line and gas line, designing
and assembling of the substrate holding arrangement, shutter
arrangement and substrate heating arrangement.

3.1.1 Vacuum System:

Vacuum system used for evaporating the films has
been shown in the Figures 3.1 and 3.2. Bell-jar made of pyrex
with 12" diameter and 12" height was used and the total body
of the Varian vacuum system was made of stainless steel
material. Variable leak valve as shown in the Fig. 3.2 was
used for admitting the precisely controlling the amount of
required gas.

Varian vacsorb pumps were used as a roughing system to attain the vacuum of less than 10^{-4} Torr. Vacsorb pumping action was achieved through the process of physical adsorption of gas molecules by chilled molecular sieve material. Therefore operation is completely free of oil contamination and vibration. Ultra high vacuum of the order of 10^{-8} Torr was obtained using vac Ion pump which provides completely clean and vibration free service. The pumping element consists of a multicell anode structure between two titanium cathode plates. Pumping was initiated by applying a high voltage (with respect to ground) between the anode and cathode. Electrons tending to flow to the anode are forced into a spiral path by the presence of magnetic field. The greately increased length of electron path results in a high probability of collision between electron and gas molecules. These collisions produce gas ions and mole electrons. Positively charged gas ions then bombard the titanium cathode plates. The bombardment knocks titanium atoms out of the plates. The sputtered titanium atoms are deposited on the anode and elsewhere forming chemically stable compounds with active gas atoms such as oxygen and nitrogen. Pump current bears a nearly linear relation to the density of gas molecules, down through the 10^{-8} Torr scale. The pump current can be read from a meter on the vac Ion pump control unit and converted to pressure with a curve provided for each pump. The meter in the vac Ion pump control unit was also calibrated to read directly on a logerithemic scale from 10^{-4} to 5×10^{-9} Torr.

The varian Dual Range Ionization Gauge Control Unit (Model No. VT971-0015) operates two types of hot filament ionization gauges to give single meter read out of vacuum system pressure from Torr (mm Hg) down to 2×10^{-11} Torr. The control unit reads pressure in the range from 1 Torr to 10^{-5} Torr with the varian Millitorr (high pressure) ionization gauge. The low pressure range is sensed by varian UHV series ionization guage. The controls for both gauges are located on the front panel of the control unit. They are color coded, yellow controls for the high pressure Millitorr gauge and blue for the low pressure gauge.

Millitorr ionization gauge is similar to other triode ionization gauges, except that the length of its electron paths is very short and emission current from filament to grid must be very low. It has a sensitivity of 0.5 Torr^{-1}. It is degassed by electron bombardment. The ion collector is a loop of tungsten wire located inside a planar grid box. Varian UHV series (low pressure) gauges give accurate pressure measurement from 10^{-3} Torr down to their X-ray limit, about 2×10^{-11} Torr. An over load circuit protecting the filaments of the vacuum gauges operates on both sides. When the pressure rises the preset value (adjustable from 10% to about 250% of the full sale reading), a negative signal will drive the trigger circuit to change the condition. Pressure relay unit will use the out-put voltage from the control unit to make or break the circuit inrelation to a set point.

3.1.2 Electron Gun And Control:

Evaporations were carried out using 2KW electron beam gun (Fig. 3.4). The power supply for electron gun was set for operation with an input power of 220V, 50Hz with maximum input current of 14 ampears during normal operation. Output voltage of 4000V (negative) d.c. unregulated and output current variable between 0-500mA was applied to the electron gun source.

Gun filaments output voltage will vary between 0-6 volts with output currents of 0-25 Ampears. Emission current knob was turned down in the counter clockwise direction to start the emission process. Hand held potentiometer connected to the remote control and rate signal receptacle on the rear panel was adjusted for evaporating the source material. Beam adjust unit (varian model no. 980-1016) may be used to change the operating voltage and shift the target area of beam impingement. For depositing uniform coating, it is important that the electron beam strikes directly on the top centre of the evaporant material kept in the crucible. The striking area can be moved by adjusting the magnetic field.

3.1.3 Chilled Water Line:

Cooling of the crucible during evaporation is very important and it was achieved by passing the chilled and filtered water through stainless steel tubing. Lay out of the water line is as shown in Fig. 3.5. Booster pump was used to

regulate the pressure of the water passing through the
electron gun. Pressure of the water was maintained at 40 PSI
as shown by meter M. Cartridge filter with brass casing was
installed in the line before the meter M as shown in Figure 3.5.
Temperature of the water was maintained at 14°C. Water line
was insulated with asbastos wool covered with teflon tape.

3.1.4 Substrate Holding Arrangement:

Figures 3.2 and 3.3 depict the sketch of chamber
parts used in electron beam evaporation. Substrate plat form
was made of stainless steel plate with 160mm diameter and
having an opening of 21 x 53 mm for fixing the mask holder.
Substrate plat form was at the height of 150mm from the
crucible. Mask holder made of copper was having a stepwidth of
1mm for keeping the masks. Molybdnum masks of 10mm diameter
with the openings of 3mm diameter and 2mm diameter were used
in the evaporation. Teflon pins were used to fix the substrate
platform on to the supporting rods of stainless steel. This
arrangement will ensure electrical insulation of the substrate
plat form. Shutter plate made of stainless steel with 0.5 mm
thickness and 30 x 60 mm size was kept below the substrate
plat form at a distance of 7.5 mm. Shutter holding rod was
fixed to the rotary motion feed through and shutter motion
was guided by the two screws fixed to the substrate plat form
as shown in the Fig. 3.3. Provision was made at the side of the
maskholder to keep the ceramic sleeve through which thermocouple
was inserted to monitor the temperature.

3.1.5   Substrate Heating Arrangement:

Substrate was radially heated using tungsten helical filament of 4" length and coil diameter of 1/4" as shown in the Figure 3.3.   Filament was kept at a distance of 10mm from the substrate platform using filament holding rods made of Aluminum. Filament supporting rods were firmly fixed to the current feed throughs made of copper rod with 16 mm diameter. Current feed through copper rods were having the current carrying capacity of 450A.   Current of 0-100 A was passed through the current feed through using (1) 100 A cable; (2) 230-15V transformer; (3) 8 A Variac. Variac was connected to the primary of the transformer as shown in Fig. 3.6.   Temperature was monitored using Alumel-Chromel thermocouple connected to the Kiethley digital multimeter through the instrumentation feed through. Reflector made of stainless steel with thickness of 0.5 mm was kept above the filament to reflect the heat on to the substrate and to prevent excessive heating of the pyrex belljar.

3.2.1   Surface Cleaning Process:

Episilicon wafers of   n and p type (Monsanto) with 1 Ohm-Cm resistivity were taken as the starting material. These had their front surface polished and back surface lapped. The sequence of steps for surface cleaning were as follows:

1.   The wafer was degreased by treating in warm trichloro-
      ethylene for about two minutes, then in warm acetone
      for two minutes to remove traces of trichloroethylene

and finally in warm methanol for two minutes to remove traces of acetone.

2. The wafer was then thoroughly rinsed in deionized water to remove all the traces of methanol.

3. Then it was transfered into a clean teflon beaker and treated with HF for 2 minutes to remove the 30-40Å thick native silicon oxide.

4. The wafer was decanted in deionized water 8 to 10 times to remove HF completely.

5. 50-60 Å thick oxide was grown on silicon wafer by pre-oxidation at 1000°C in dry oxygen ambient. Oxygen flow rate was kept slightly greater than 1600 cc/minute and oxidation time was 10 minutes.

6. The grown oxide was then etched by treating the wafer with HF for 3 minutes.

7. The wafer was finally rinsed in deionized water thoroughly.

After this chemical cleaning silicon wafer should be hydrophobic (test). Otherwise the whole procedure should be repeated. Steps 5 and 6 were employed to remove minor mechanical defects and some of the diffused impurities at the surface.

3.2.2 Oxidation of Silicon Wafers:

For heterojunctions, interfacial oxide layer of about 20Å thickness was grown at 700°C in about 1 minute time. For TCOS devices thick oxide of about 125Å was grown in dryoxygen

at 900°C and oxidation time was 40 minutes. In all these oxidation processes flow rates were maintained at 1.6 liters/ minute and Thermco-Sparten furnace was used.

3.2.3 Electron Beam Evaporation of In_2O_3/SnO_2:

Evaporation material was indium tin oxide in the tablet form (Atomergic Corporation). It was cleaned with warm TCE and warm methanol before loading into the electron beam crucible. Fused silica wafer (ESI 1) was kept on the copper substrate holder with the central circular opening of 7 mm ; n-type epi silicon (ENI 1) and p-type epi silicon (EPI 1) were kept on the same copper substrate holder with an opening of 7 mm. Vacsorb pumps were used to obtain the rough vacuum of 10^{-4} Torr and initial vacuum was monitored using thermocouple gauge. Using vac Ion pumps pressure was brought to 1×10^{-6} Torr before starting evaporation. Substrate temperature during evaporation was maintained at 298°C, as measured by the Kiethley digital multimeter. Hand held potentiometer (remote control) was kept at 4.0 during evaporation. Emission maximum position was kept at 70 through out evaporation. Evaporation time was 45 minutes (with 3 cycles of 15 minutes each) . During evaporation pressure was less than 10^{-5} Torr.

3.2.4 Annealing of the Samples:

Annealing of the samples ESI 1, ENI 1 and EPI 1 was carried out in semiconductor Devices Laboratory in CVD furnace using annealing tube. Annealing ambient was oxygen and a flow

rate of 1000 cc/minute was maintained. ESI 1 was annealed at a temperature of 300°C for 1 hour; ENI 1 was annealed at 300°C for 2 hours and annealing of EPI 1 was carried out at 400°C for 1 hour.

3.3 Electrical Characterization:

3.3.1 Measuring Conductivity-Type:

The deposited film was subjected to a test in which a hot probe was pressed on some point on the film and cold probe on some other point. The direction of deflection of the spot of light on the graduated scale of leads and Northrup galvanometer was noted. The direction of deflection indicated the conductivity type of the deposited film.

3.3.2 Resistivity measurement:

A four point probe was used for measuring the resistivity of the deposited film. The curcuit arrangement for this consisted of a power supply connected accross the outer probes in series with an ammeter. The voltage across the inner probes was measured by a differential Fluke 803 B AC-DC voltmeter.

To start with, the voltmeter was adjusted for null deflection by placing the meter in the position " Calibrate" and adjusting the pointer to read zero. The probes were pressed against the sample so that all the four probes made good contact with it Current was measured insteps of 1mA by adjusting the voltage from the proce supply. In each case the voltmeter was balanced for null deflection by tuning the knobs provided for this

purpose and the voltage was read off directly corresponding to the position of knobs.

Voltage versus current was plotted and the slope of the straight line determined the ratio $\frac{V}{I}$. The sheet resistivity of the film, R_s (ohms per square) was calculated using the formula;

$$R_s = \underline{\quad\quad} = 4.532 \left(\frac{V}{I}\right) \quad / \quad ,$$

where   is the sheet resistivity of the film and 't', the thickness. By knowing the thickness, the resistivity was calculated using the formula

$$= R_s \quad t. \text{ Ohm-cm},$$

3.4   Structural Characterization:

3.4.1   X-ray Characterization:

X-ray diffraction supplements electron diffraction in the determination of the crystallographic film structure. By use of a goniometer and counter, lattice spacings and intensities can be determined with considerably higher accuracy, but greater film thickness and longer exposure times are required than for electron diffraction. The deposited films were mounted on an X-ray crystal diffractometer. The samples were scanned by using copper Kalpha radiation in the range from $0°$ and $100°$. The data obtained were traced by a recorder which moves inresonance with the rotation of X-ray diffractometer. The movement on the

chart on the recorder was kept at 2° per minute and the intensity was kept in the range of 1000 CPS. A record of the X-ray diffraction pattern (intensity Vs 2 0) was obtained for different films. Electron beam evaporated films may consist of more than one phase and identification of such phases is important since they will have influence over the properties of the film.

3.4.2 Transmission Electron Microscopic Characterization:

Transmission microscopy requires film thicknesses of the order of 100 to 1000 Å. Indium oxide/Tin oxide films are not attacked by most of the strong acids and bases. In_2O_3/SnO_2 films deposited on silicon were treated with dilute HF solution. HF will etchout the silicon oxide. After treating with HF, films were rinsed with deionized water 4 to 5 times. The films were broken into small portions and the floating films were carefully picked by the copper grids. Specimans suitable for TEM observation were examined by TEM operating at 100 KV accelarating voltage. The samples were seen in both transmission and diffraction modes and photographed. The micrographs were taken at different magnifications.

Selected area diffraction is a powerful tool for identifying and studying the orientation of microscopic crystallites, twins, included grains, subgrains, precipitates, and transformation products. The diffraction pattern of the film can give an idea of the nature of the film namely whether

the film is crystalline, polycrystalline or amorphous. The amorphous films are characterized by diffused rings. Crystalline films are characterized by strong diffraction spots. The radii of the rings in the polycrystalline film are related to the interplanar spacing by

$$Rd_{hkl} = L$$

where R is the radius of any ring on the diffraction pattern and L, the camera constant. By measuring the radii of the diffraction rings of a standard gold pattern whose interplanar spacings are known, the camera constant is determined. The radii of the ring pattern of the given film is then measured and the corresponding d_{hkl} evaluated. The diffraction rings are then indexed.

4. RESULTS AND DISCUSSION :

4.1 Electrical Characterization:

The conductivity type of all the evaporated samples was found to be strongly n type.

Table 4.1 indicates the sheet resistivities of the films evaporated on fused silica substrate, n type and p type silicon substrates. Annealing conditions were different for different samples. ESI 1 was annealed at 300°C for 1 hour, ENI-1 was annealed at 300°C for 2 hours and EPI 1 was annealed at 400°C for 1 hour. Annealing ambient was oxygen in all the cases. Sheet resistivity of LSI 1 was 124   , ENI 1 was 102   and EPI 1 was 90   . From the interference colors of all these films which was blue/ tan, thickness was found to be 1100Å. As the film thickness was about the same for all the samples, difference in sheet resistivity among these samples might be attributed to the difference in the annealing conditions. Oxidation conditions were not optimized in this case. Annealing temperature was varied between 300 - 400°C . With the pyrex tube used, annealing temperature could not exceed above 400°C.

Photovoltages were measured both for electron beam evaporated and sputtered films on n and p type. Significant photovoltage was measured on n type while none on p type in the case of electron beam evaporated films which was in contrast to the sputtered films. Hence large barrier formed on n type in

the case of electron beam evaporated films. High barrier height
was obtained on p type than on n type in the case of sputtered
films.

4.2 Structural Characterization:

4.2.1 X-ray Characterization:

X-ray diffractograms of indium oxide films
evaporated on the silica substrates were obtained by using
copper K alpha radiation. Many strong diffraction peaks were
obtained and that indicates the polycrystalline nature of the
film. X-ray diffractogram contained more peaks in addition to
that of In_2O_3 films and this indicates the presence of second
phase in In_2O_3 films. Second phase elements present in the
film were found to be Sn_3O_4 and SnO_2. To analyze all the diff-
raction peaks range was changed from 1000 CPS to 10,000 CPS.
Goniometer speed was kept constant at 2" per minutes, time
constant was maintained at 2, chart speed was 1" per minute and
starting angle was 10°. Scanning of the diffractogram peaks
was done upto the angle of 90°. Stronger peaks of silicon
substrate were observed at 5000-10,000 CPS range. The peaks
of x-ray diffractogram are indexed as shown in Table 4.2.

4.2.2 TEM Analysis:

The transmission electron diffraction patterns
were obtained for In_2O_3 films evaporated on fused silica wafer.
Film was analyzed at different regions. Selected area diffraction
patterns as shown in the Fig. 4.1 indicates the polycrystalline

nature of the film. From the micrographs as shown in the Fig. 4.2, grain size was obtained which was in the range of 1000 to 3000Å . Micrographs have been shown in the Fig. 4.3 at different magnifications.

4.3 General Observations of the Electron Beam Evaporated Films:

Feng et.al.[24] have deposited indium tin oxide (ITO) films on ntype silicon by electron beam evaporation of a mixture of 90:10 molar% In_2O_3: SnO_2 powder. ITO was deposited at a rate of about 10Å/Sec to a thickness of about 1000 Å. In their evaporation substrate heating was not employed but the films were heat treated in air at 350°C for 30 minutes. ITO films on glass before the heat treatment were reported to be black in color. Feng et.al[25] have evaporated SnO_2 by an Airco electron-beam source placing SnO_2 powder on a graphite liner. Here also no substrate heating was employed during the deposition. Tin oxide was deposited to a thickness of 1000Å, resulting in blue color. After deposition of the tin oxide, coated silicon substrate was heated in air at 300°C for 1 hour. Electron beam deposited films were amorphous before the heat treatment and after the heat treatment films have become polycrystalline in nature as observed by their x-ray diffraction pattern. Feng et.al.[26] have e-beam deposited SnO_2 films at room tempera- ture. Films were highly resistive and yellowish color before heat treatment and they became more conductive and transparant after heat treatment.

Here author has used tin-doped indium oxide in the
tablet form and substrate heating was employed during evaporation.
In the case of ESI 1 film was opaque and nonuniform before
annealing and after annealing the film has become transparant.
In the case of ENI 1 film appeared to be opaque and with gray
color before annealing and after annealing the film was very
reflecting, shining blue/tan. In the case of EPI 1 film was
opaque, grayish in color, non reflecting and soft before
annealing and the film has become very much reflecting with
blue/tan color. Generally it was observed that films were
opaque before annealing and after annealing they have become
transparant. Transparancy was about 92% in these films after
annealing. Good quality films were obtained by substrate
heating.

Table 4.1

	ESI 1	ENI 1	EPI 1
1. Sample Number	ESI 1	ENI 1	EPI 1
2. Sample size and Shape.	10mm ∅ wafer.	7mm x 7mm	7mm x 7mm
3. Starting Material	Fused Silica Wafer	N type epi silicon	P type epi silicon
4.a.Annealing Ambient	Oxygen, 1000 cc/Min	Oxygen, 1000 cc/Min	Oxygen, 1000 cc/Min.
b.Annealing Temperature.	300°C	300°C	400°C
c.Annealing Time	1 hour	2 hours	1 hour.
d.Furnace	In SDL Lab., CVD furnace, Annealing tube.	In SDL Lab. CVD furnace, Annealing tube.	In SDL Lab. CVD furnace, Annealing tube.
5. Conductivity type.	Film Highly N type	Film Highly N type	Film Highly N type
6. Sheet resistivity (R_g)	124	102	90

Table 4.2

Calculated X-ray Reflection for In_2O_3 Films.

Cu Kalpha $= 1.5418$ Å

S.No.	2θ	θ	2 Sinθ	$d = \dfrac{\text{(Å)}}{2Sin\theta}$	Standard d	hkl
1.	28.2	14.1	0.48723	3.1646	3.138 (Si)	(111)
2.	30.4	15.2	0.5244	2.9401	2.921 (In_2O_3)	(222)
3.	31.3	15.65	0.5395	2.8578	2.818(Sn_3O_4)	
4.	32.7	16.35	0.5630	2.7385	2.704(In_2O_3)	(321)
5.	33.9	16.85	0.5797	2.6596	2.644(SnO_2)	(101)
6.	35.7	17.85	0.6131	2.5148	2.529(In_2O_3)	(400)
7.	40.4	20.2	0.6906	2.2326	2.237(Sn_3O_4)	
8.	42.3	21.15	0.7330	2.1034	2.066(In_2O_3)	(422)
9.	44.3	22.15	0.7541	2.0446	2.120(SnO_2)	(210)
10.	45.7	22.85	0.7766	1.9853	1.984(In_2O_3)	(431)
11.	46.0	23.0	0.7815	1.9729		
12.	47.0	23.5	0.7975	1.9333	1.920(Si)	(220)
13.	47.4	23.75	0.8055	1.9141	1.848(In_2O_3)	(521)
14.	52.8	26.4	0.8893	1.7337	1.735(In_2O_3)	(530)
15.	54.35	27.18	0.9134	1.6880	1.686(In_2O_3)	(600)
16.	55.20	27.6	0.9266	1.6639	1.659(B Sn)	(301)

S.No.	2θ	θ	$2Sin\theta$	$d = \dfrac{1}{2Sin\theta}(\overset{\circ}{A})$	Standard	hkl
17.	56.10	28.05	0.9405	1.6393	1.638(Si)	(311)
18.	57.10	28.55	0.9559	1.6129	1.600(In_2O_3)	(620)
19.	61.50	30.75	1.0226	1.5077	1.492(In_2O_3)	(631)
20.	65.70	32.85	1.0849	1.4212	1.431(In_2O_3)	(545)
21.	66.20	33.10	1.0922	1.4117	1.403(In_2O_3) or 1.415(SnO_2)	(640) or (301)
22.	69.10	34.55	1.1343	1.3593	1.357(Si)	(400)
23.	74.1	37.05	1.2050	1.2795	1.285(In_2O_3)	(732)
24.	75.40	37.70	1.2231	1.2606	1.265(In_2O_3)	(800)
25.	76.10	38.05	1.2327	1.2508	1.246(In_2O_3) or (Si)	(811) or (331)

Table 4.3

Transmission Electron Microscopic Diffraction Data:

Material	Ring No.	Radius 'R' in mm	$d_{hkl}(\overset{\circ}{A})$	Camera Constant $L=Rd_{hkl}$ ($\overset{\circ}{A}_{mm}$)	Average L ($\overset{\circ}{A}$ mm)
	1.	13.0	2.355	30.615	
	2.	15.0	2.039	30.585	
Gold	3.	21.0	1.442	30.282	30.481
	4.	24.75	1.230	30.4425	

Table 4.3

Transmission Electron Microscopic Diffraction Data:

Material	Spot No.	Radius 'R' in mm	Camera Constant $L(\overset{o}{A}mm)$	$d_{hkl} = \dfrac{L(\overset{o}{A})}{R}$
	1	7	30.481	4.3544
	2	10	30.481	3.0481
	3	11.5	30.481	2.6505
	4	12.5	30.481	2.4385
In_2O_3	5	13.5	30.481	2.2579
	6	14.75	30.481	2.0665
	7	16.5	30.481	1.8473
	8	18.0	30.481	1.6934
	9	19.5	30.481	1.5631

5. CONCLUSION:

Vacuum chamber parts were designed and assembled for carrying out the electron beam evaporation. This included the design and assembling of the substrate holding arrangement, shutter arrangement, laying of the chilled water line for cooling the electron gun crucible and laying of the gas line for purging the water. All the designed systems were found to perform satisfactorily. Tin doped indium oxide films, evaporated by electron beam evaporation using the above set-up, were having satisfactory optical transparancies and sheet resistivities. In the case of electron beam evaporated films, significant photovoltage was observed on n-type silicon compared to none observed on p-type silicon. This was in contrast to the sputtered films.

Even when the film thickness was same, there was variation in the sheet resistivity for different samples. This may be due to the variation in the annealing parameters. Good quality films were obtained at 300°C using ITO tablet. Substrate heating during evaporation was not tried for the electron beam evaporated films in earlier investigations.

Transparancy of the tin doped indium oxide films, was increased considerably by annealing the samples in the oxygen ambient at 300-400°C. Transparancy measured was about 92%. X-ray characterization has indicated the presence of second phase elements in the In_2O_3 film. Diffractometer peaks revealed the polycrystalline nature of the film. Selected area

diffraction patterns   obtained in TEM characterization has confirmed the polycrystalline nature of the films

Charge material form is very important   in the electron beam evaporation. In the present work tin doped indium oxide was used in the tablet form.

LIST OF REFLRENCES:

1. Z. Jarzebski, Oxide Semiconductors, Pergamon,
    New York, 1979.

2. K.L. Chopra, Thinfilm Phenomena, McGraw-Hill,
    New York, 1969.

3. J.E. Varger and W.A. Bailey, " Evaporation, Sputtering
    and Ion plating," Solid State Technology, 15, 79 (1973).

4. J.E. Varger and W.A. Bailey," Thinfilm vacuum Equipment,"
    Solid State Technology. 15, 93 (1973)

5. Hand Book of Thinfilm Technology, McGraw-Hill,
    New York, 1970.

6. Edwards, B. Graper, J. Vac. Sci. & Tech. 8, 333 (1971).

7. S. Furuuchi and H. Sakater, Jap. J. Appl. Phys.
    13, 1905 (1974).

8. T. Wiktorezyk and C. Wesokowska, Thin Solid Films,
    71, 15 (1980).

9. D. Hoffman and D. Leibowitz, J. Voc. Sci. & Tech.
    8, 107 (1971).

10. D. Hoffman and D. Leibowitz, J, Vac. Sci. & Tech.
    9, 326 (1972).

11. Edward B. Graper, J. Vac. Sci. & Tech.
    7, 282 (1970).

12. Freitz L. Schvermeyer, J. Appl. Phys.
    13, 5856 (1971).

13. S.M. Sze, Physics of Semiconductor Devices,
    Wiely, 1969.

14. J. Kontecky, J. Phys. Chem. Solids.
    14, 233 (1960).

15. D. Pugh, Phys. Rev. Latters.
    12, 390 (1964).

16. S. Kar, S. Varma and P. Saraswat, J. Appl. Phys.
    53, X (1982).

17. M. Nagasawa and S. Shinoyo, Japan. J. Appl. Phys. 10, 472 (1971).

18. E. Leja and A. Kolodziej, Thin Solid Films. 67, 45 (1980).

19. S. Kar, S. Ashok and S.J. Fonash, J. Appl. Phys. 51, 3417 (1980).

20. S. Kar and W.E. Dahlke, Solid-State Electron. 15, 869 (1972).

21. S. Kar, J. Appl. Phys. 49, 5278 (1978).

22. A.N. Saxena, Surface Science. 13, 151 (1969).

23. S. Ashok, J.M. Borrego and R.J. Guttamann, Solid-State Electron. 22, 621 (1979).

24. Tom Feng, Amal K. Ghosh and Charles Fishman, J. Appl. Phys. 50, 4972 (1979).

25. Tom Feng, Amal K. Ghosh and Charles Fishman, J. Appl. Phys. 50, 8070 (1979).

26. Tom Feng, Amal K. Ghosh and Charles Fishman, Thirteenth IEEE Photovoltaic Specialists Conference, 519 (1978).

FIGURE CAPTIONS

Fig. 2.1   SoS diode on n-type at a moderate forward bias.

Fig. 2.2   Basic equivalent circuit incorporating surface
                state.

Fig. 2.2(b)   Equivalent circuit showing frequency dependent
                capacitance C_p in parallel with frequency
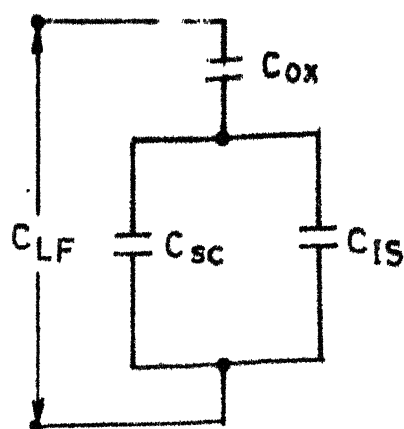   dependent conductance.

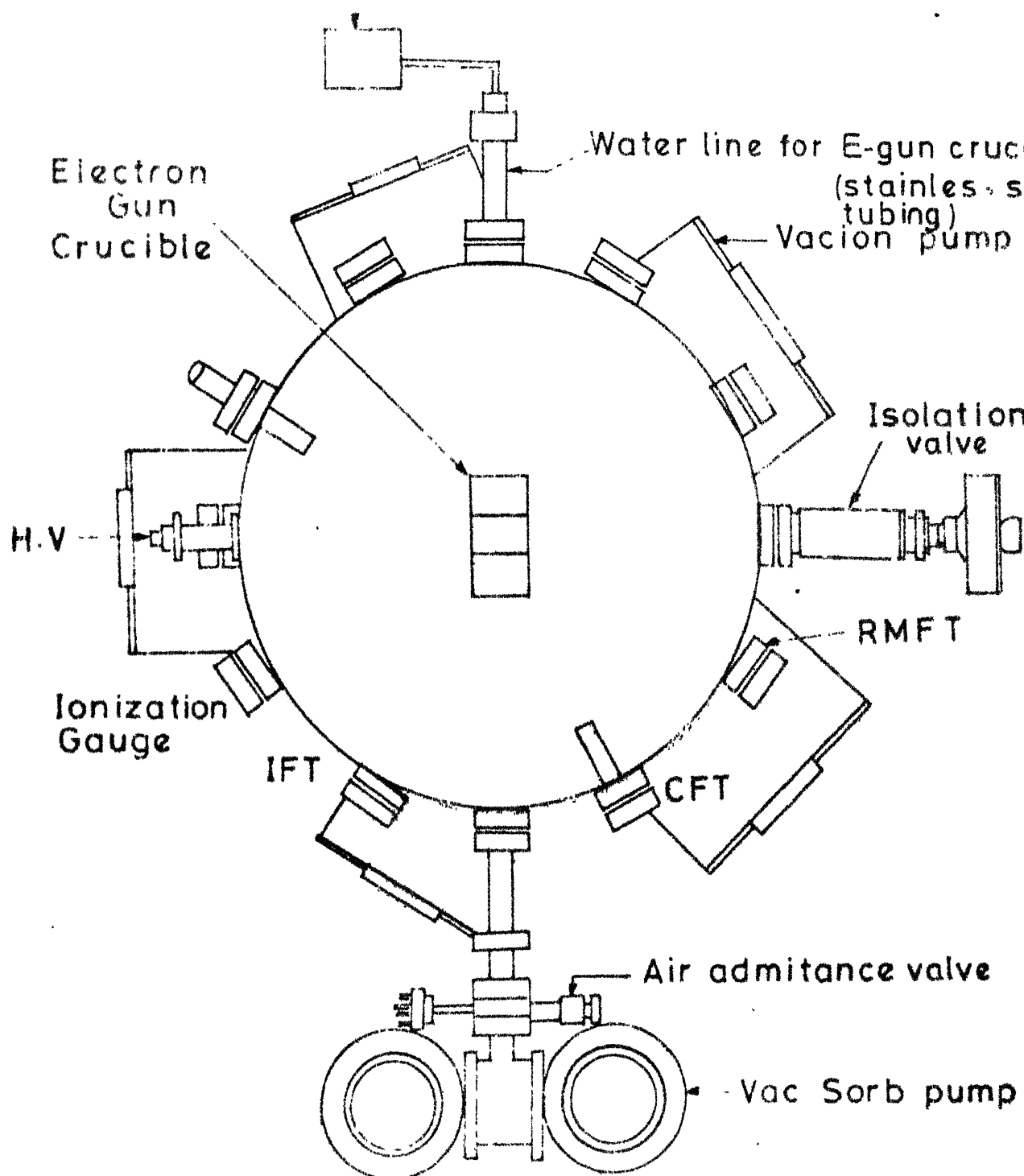Fig. 2.3   Equivalent circuit at low frequency.

Fig. 3.1   Top view of the varian vacuum chamber
                (without sustrate platform).

Fig. 3.2   Sketch showing chamber parts.
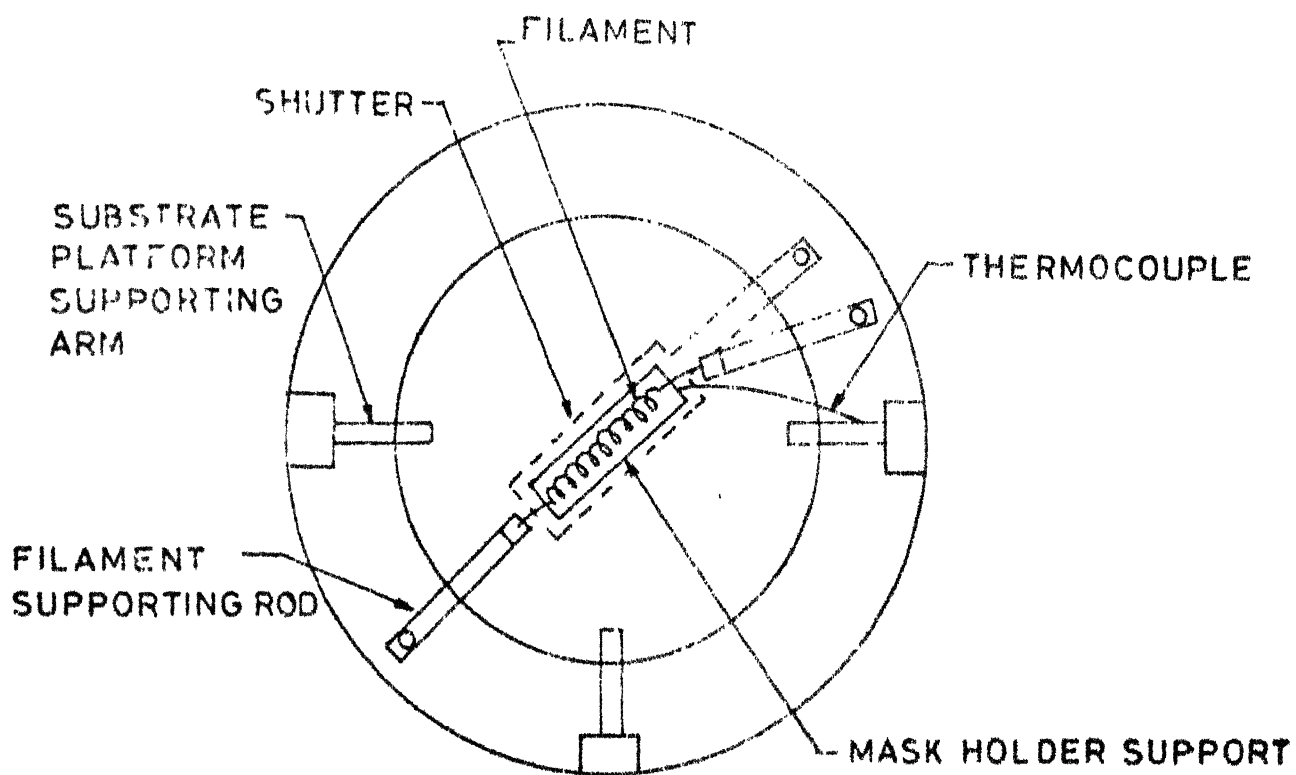
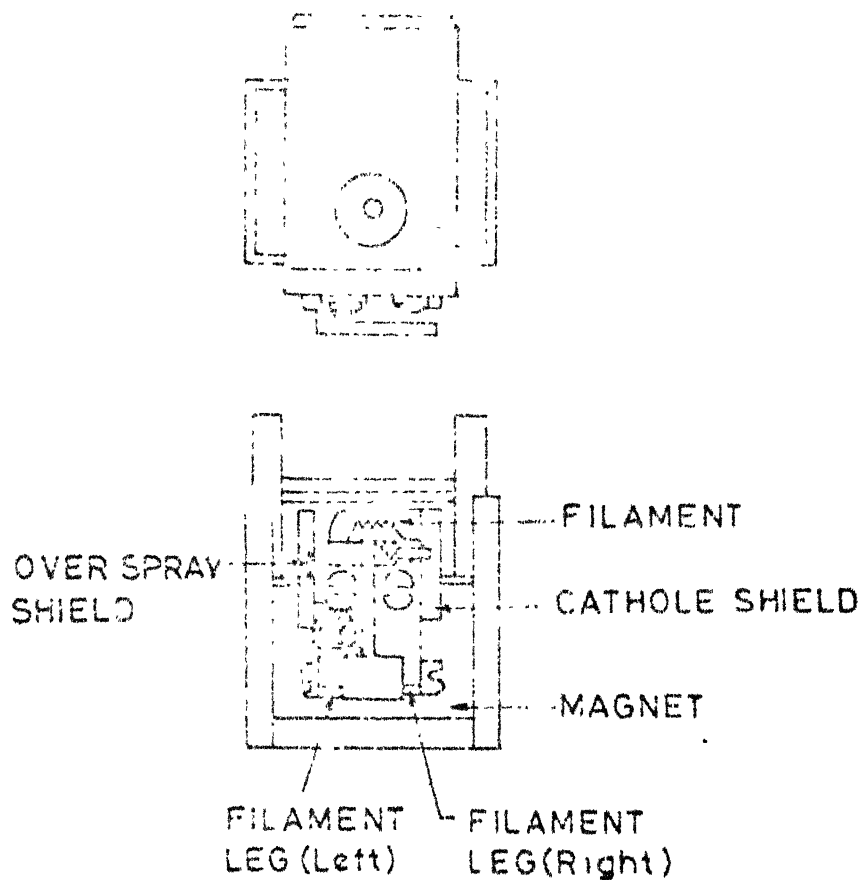Fig. 3.3   Top view of substrate platform (without
                retlector).

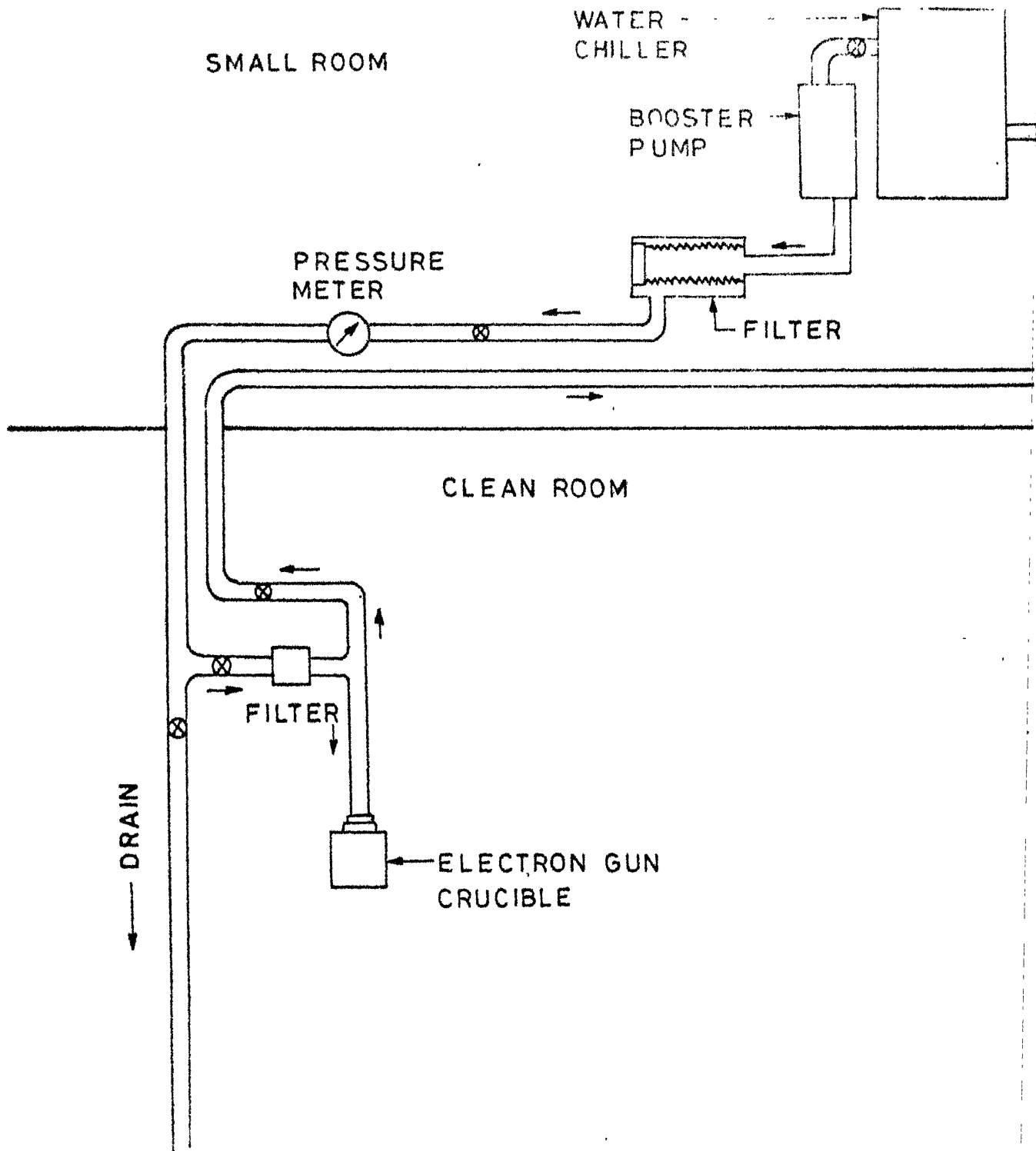Fig. 3.4   Schematic diagram of 2kW electron gun head.
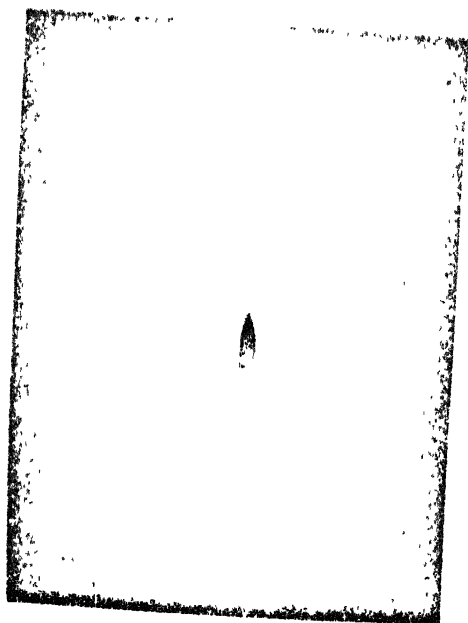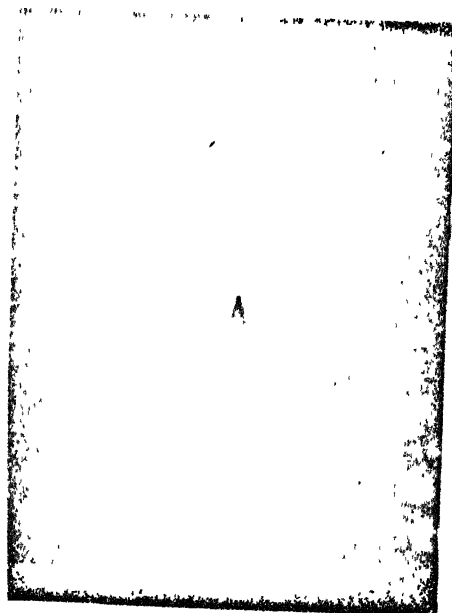
Fig. 3.5   Water line layout.

Fig. 3.6   Substrate heating system.

Fig. 4.1   Selected area diffraction patterns.

Fig. 4.2   Micrographs at magnifications 17000 and 22,000

Fig. 4.3   Micrographs at magnifications 5,100; 7,800;
                63,000 and 1,300.
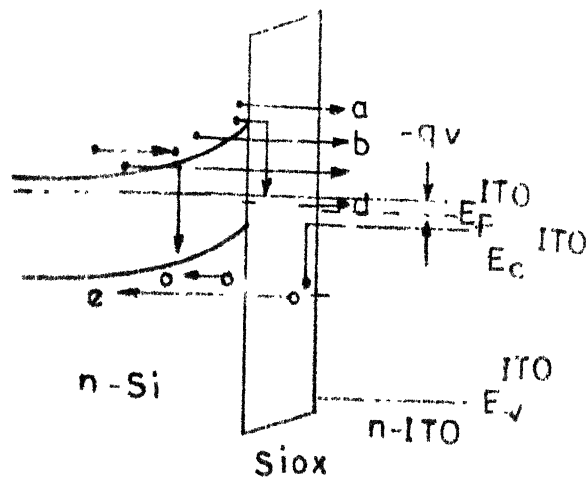
Fig. 2·1 SOS diode on n type at a moderate forward bias
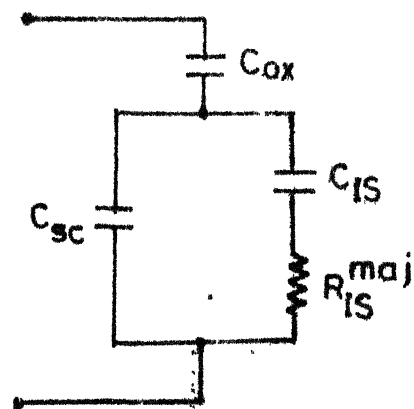
Fig. 2·2 (a) Basic equivalent circuit incorporating surface states
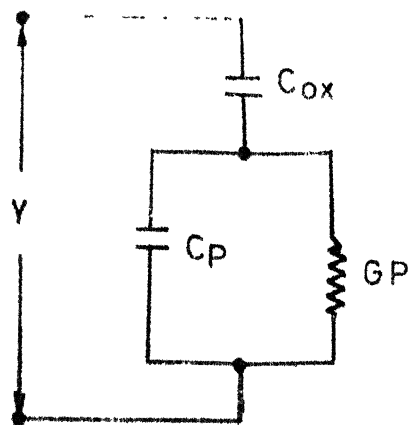
Fig. 2·2b Equivalent circuit showing frequency
dependent capacitance C_P in parallel
with frequency dependent conductance

Fig. 2·3 Equivalent circuit at low frequency

Water line layout (shown in Fig. 3.)

Water line for E-gun cruci
(stainless s
tubing)

Electron
Gun
Crucible

Vacion pump

Isolation
valve

H.V

RMFT

Ionization
Gauge

IFT

CFT

Air admitance valve

Vac Sorb pump

Fig. 3.1 Top view of the varian vacuum
chamber (without sustrate platform)
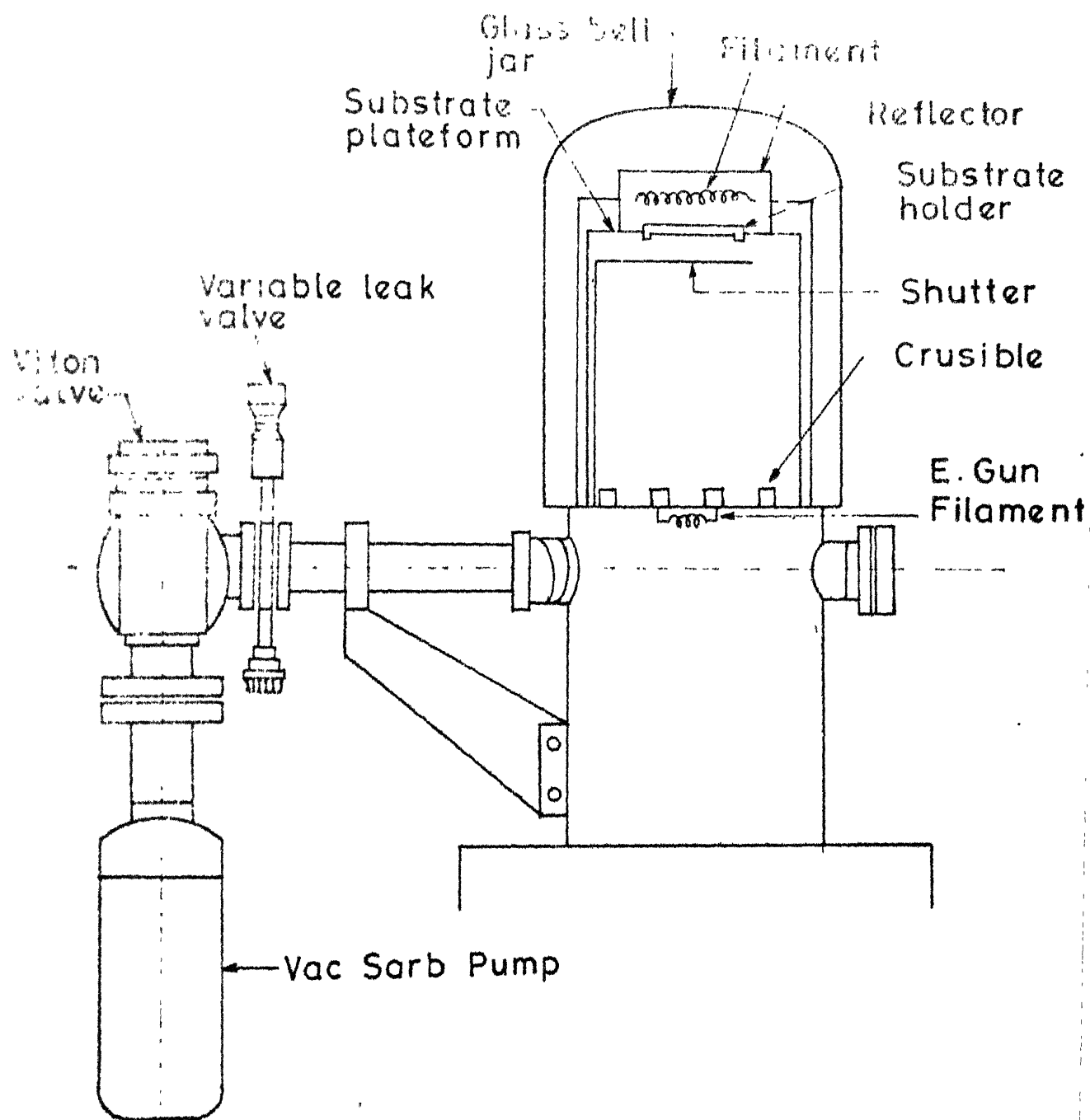
Fig. 3·2 Sketch showing chamber parts

FIG·3·3 TOP VIEW OF SUBSTRATE PLATFORM
(Without reflector)

FIG. 3·4 SCHEMATIC DIAGRAM OF 2kW ELECTRON GUN HEAD

FIG 3·5 WATER LINE LAYOUT

VOLTAGE
STABILIZER

MAIN
POWER

8 AMPS
VARIAC

230 V -15 V
TRANSFORMER

CFT

CFT
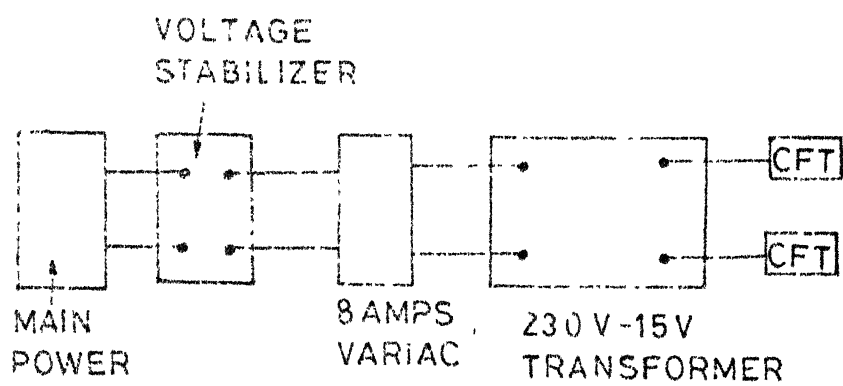
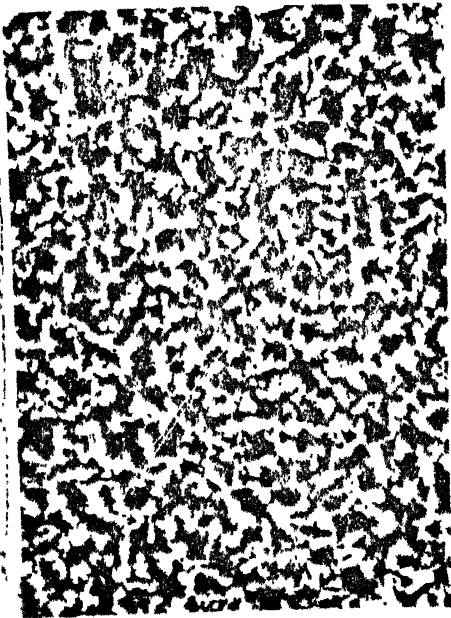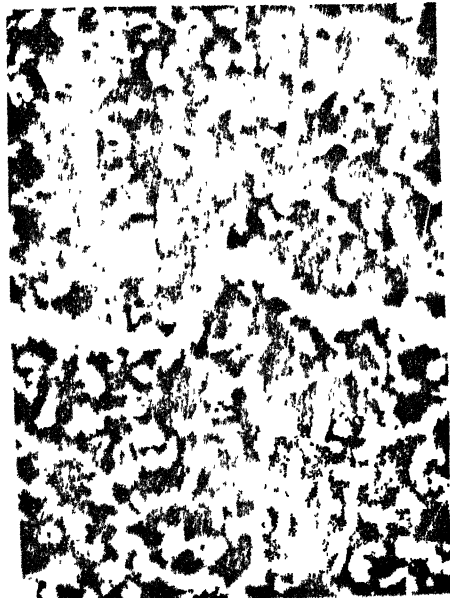FIG. 3·6 SUBSTRATE HEATING SYSTEM

Gold

In_2O_3

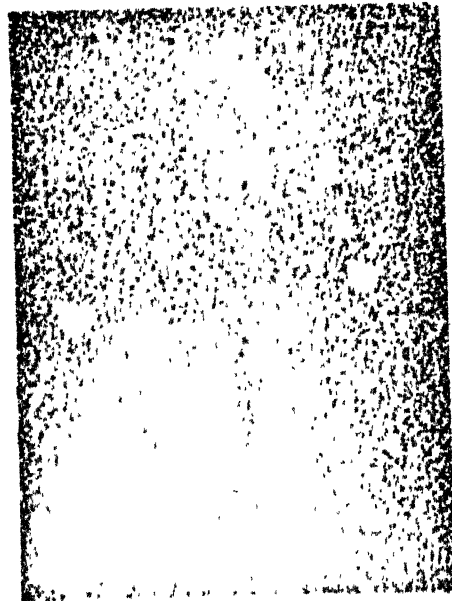In_2O_3

Fig. 4.1 - Selected Area Diffraction Patterns.

X 5,100

X 7,800

X 63,000

X 1,300

Fig: 4.3 - TEM Micrographs at Different Magnifications.

MS-1982-N-BAB-PRE